

STRUCTURE OF NEUTRON STAR ENVELOPES

E. H. GUDMUNDSSON

Nordita, Copenhagen; and Science Institute, University of Iceland, Reykjavik

C. J. PETHICK

Nordita, Copenhagen; and Department of Physics, University of Illinois at Urbana-Champaign

AND

R. I. EPSTEIN

Nordita, Copenhagen

Received 1982 November 8; accepted 1983 February 10

ABSTRACT

We have investigated the envelopes of nonmagnetic neutron stars using the best available opacities and equation of state. The temperature at the inner boundary of the envelope, T_b , is found to be very nearly a universal function of the parameter T_s^4/g_s , where T_s is the effective surface temperature, and g_s is the surface gravity of the neutron star. This result is used to derive a number of other scaling relations, to investigate the effects of general relativity on the thermal structure of the envelope, and to compare envelope calculations by different workers. Tests of the sensitivity of the computations to variations of the input physics show that the accuracy of the T_b versus T_s relation depends largely on having accurate values for the conductive opacity in the region where it is dominated by electron-ion scattering. In our calculations we use the conductive opacities calculated by Yakovlev and Urpin, which are the most accurate ones available. For a given T_b we find luminosities that are 2–2.5 times lower than those calculated using Flowers and Itoh's calculations of the conductive opacities.

Subject headings: dense matter — relativity — stars: interiors — stars: neutron

I. INTRODUCTION

The first calculations of the cooling of neutron stars were performed almost 20 years ago (Chiu and Salpeter 1964; Morton 1964; Tsuruta 1964). In the intervening years a number of additional models were calculated, for example, by Tsuruta and Cameron (1966), Tsuruta (1974), Malone (1974), and Maxwell (1979) (see also the reviews by Tsuruta 1979, 1980), and most recently, results obtained using the *Einstein Observatory* and other X-ray satellites stimulated a spate of activity in this field (e.g., Urpin and Yakovlev 1979; Glen and Sutherland 1980; Van Riper and Lamb 1981; Tsuruta 1981a; Nomoto and Tsuruta 1981; Richardson *et al.* 1982).

The neutron star X-ray luminosities (or the upper limits on the X-ray luminosities) measured by the *Einstein Observatory* (see, e.g., Helfand, Chanan, and Novick 1980; Helfand 1981a, b) are in some cases comparable with those derived from the recent theoretical cooling calculations for neutron stars without pion condensates. However, the various cooling calculations give rather different results, with the surface luminosities differing in some cases by an order of magnitude or more for seemingly similar models. Pinpointing the reasons for the differences between the calculations is difficult because different workers often use different input physics for the equation of state, neutrino emissivities, specific heats and opacities and usually choose different stellar masses when reporting results.

There are two rather different and separate problems involved in the study of neutron star cooling. One is the thermal evolution of the high-density core, which contains nearly all the mass and heat content of the star, and the second is the thermal structure of the envelope, i.e., the outer region of the star where densities are less than 10^{10} – 10^{11} g cm⁻³. In this paper we shall concentrate on the second problem. We will show, among other things, that it is possible to gain valuable insights into cooling calculations by studying neutron star envelopes separately from the specific hydrostatic and thermal structure of the stellar cores. Calculations similar in spirit to ours have previously been reported by Urpin and Yakovlev (1979).

The structure of the paper is as follows: In § II we discuss the general relativistic equations of the structure and evolution of nonmagnetic neutron stars and show that they can be reduced to a single equation for calculating the thermal structure of neutron star envelopes. The physical input, i.e., the equation of state and the opacity, needed to solve the thermal structure equation is investigated in § III, and § IV contains the numerical results of our envelope model calculations. There we also show that the thermal structure of neutron star envelopes is determined by the single parameter T_s^4/g_s , where T_s is the effective surface temperature, and g_s is the surface gravity of the star. This important result is used in § V to derive a number of other scaling relations. In § VI we investigate in detail the effects of

general relativity on the envelope thermal structure, and in § VII we present the results of a sensitivity analysis which pinpoints the regions in which it is most important to know the opacity well in order to obtain a reliable relationship between the temperatures at the outer and inner boundaries of the envelope. The results of our envelope calculations are compared with those of other workers in § VIII, and § IX gives a short summary of our major conclusions.

II. THE THERMAL STRUCTURE EQUATION

The hydrostatic equilibrium and thermal evolution of spherically symmetric, nonrotating, and nonmagnetic neutron stars are determined by six ordinary differential equations (eqs. [4]–[9]), which are the relativistic generalizations of the Newtonian equations of stellar structure and evolution. In a fully dynamical calculation of neutron star thermal evolution these equations must be solved numerically for each specific neutron star model. This is generally a very time-consuming and costly procedure, but the problem can be simplified considerably by dividing the neutron star into two regions which can be studied separately: the high-density interior, which we shall call the core, containing practically all the mass and thermal energy of the star, and an insulating envelope, which surrounds the core and which has no sources or sinks of energy. For sufficiently old stars the redshifted temperature (Te^{Φ/c^2}) in the core is uniform, whereas temperature gradients can be appreciable in the envelope.

In this section we will show that for most neutron stars more than a few tens of years old, the full set of general relativistic equations can to a very good degree of approximation be reduced to a single equation in the envelope. This equation, which determines the thermal structure of the envelope, can be written as

$$\frac{dT}{dP} = \frac{3}{16} \frac{\kappa}{T^3} \frac{T_s^4}{g_s}, \quad (1)$$

where T is the temperature, P is the total pressure, κ is the total opacity of the stellar matter, T_s is the effective surface temperature, and

$$g_s = \frac{GM}{R^2} e^{\Lambda_s} \quad (2)$$

is the proper surface gravity of the star (i.e., the acceleration due to gravity as measured on the surface). In equation (2) G is the Newtonian gravitational constant, M and R are the gravitational mass and radius of the star, respectively, and e^{Λ_s} is the surface value of the relativistic length correction factor

$$e^{\Lambda} = \left(1 - \frac{2Gm}{c^2 r}\right)^{-1/2}, \quad (3)$$

where c is the velocity of light, r is the Schwarzschild radial coordinate, and $m(r)$ is the gravitational mass enclosed within a sphere of radius r .

Inspection of equation (1) shows that the thermal structure of neutron star envelopes is determined by the

two parameters g_s and T_s . Models of neutron star envelopes can therefore easily be calculated and classified in terms of the surface gravity and the surface temperature, independently of the specific structure of the cores. In fact, in § IV we shall demonstrate that the thermal structure is largely determined by the single parameter T_s^4/g_s . We also note that the effects of general relativity enter only through the expression for the surface gravity of the star (eq. [2]).

To derive equation (1) we use the six general relativistic equations, equations (4)–(9). For a more detailed discussion of these equations see, for example, Thorne (1967). For our purposes the most important of these equations are the Tolman–Oppenheimer–Volkoff (TOV) equation of hydrostatic equilibrium and the energy transport equation. The first is

$$\frac{dP}{dr} = -\left(\rho + \frac{P}{c^2}\right) \frac{G(m + 4\pi r^3 P/c^2)}{r^2} e^{2\Lambda}, \quad (4)$$

where ρ is the mass-energy density, and the other symbols are defined above. The heat transport equation is

$$\frac{d(Te^{\Phi/c^2})}{dr} = -\frac{3}{16\sigma} \frac{\kappa\rho}{T^3} \frac{L_d}{4\pi r^2} e^{\Phi/c^2} e^{\Lambda}, \quad (5)$$

where σ is the Stefan–Boltzmann constant, L_d is the luminosity due to thermal conduction and radiation, e^{Φ/c^2} is the redshift factor, and Φ is the gravitational potential, which is determined by the source equation

$$\frac{d\Phi}{dr} = \frac{G(m + 4\pi r^3 P/c^2)}{r^2} e^{2\Lambda}. \quad (6)$$

There is no corresponding transport equation for the neutrinos since at the temperatures of interest to us here ($T \lesssim 10^9$ K), their mean free path is of the order of one or more stellar radii, and hence they act simply as a sink of energy and do not transport energy from one part of the star to another. The equation for the neutrino luminosity, L_ν , is

$$\frac{d(L_\nu e^{2\Phi/c^2})}{dr} = \epsilon_\nu e^{2\Phi/c^2} 4\pi r^2 e^{\Lambda}, \quad (7)$$

where ϵ_ν is the neutrino emissivity per unit volume. In this investigation we are interested in nonaccreting neutron stars. In these stars there is no nuclear burning, and the equation of energy conservation can be written as

$$\frac{d(L e^{2\Phi/c^2})}{dr} = -c_\nu \frac{dT}{dt} e^{\Phi/c^2} 4\pi r^2 e^{\Lambda}, \quad (8)$$

where L is the net luminosity and is equal to $L_d + L_\nu$; c_ν is the specific heat per unit volume; and t is the time measured by an observer at $r = \infty$, who is at rest with respect to the star.

Finally, the equation which determines the gravitational mass, m , enclosed within a sphere of radius r is

$$\frac{dm}{dr} = 4\pi r^2 \rho. \quad (9)$$

In the above equations the quantities P , ρ , T , κ , L , L_d , L_v , c_v , and ϵ_v are all local ones, i.e., they are evaluated in a proper reference frame comoving with the stellar material.

The boundary conditions at the center are $m(0) = L(0) = L_v(0) = 0$. As an outer boundary condition we use the Eddington approximation and define the surface pressure, P_s , to be that at an optical depth of $\frac{2}{3}$, i.e., $P_s = \frac{2}{3}g_s/\kappa_s$, where κ_s is the value of the opacity at the surface. The effective surface temperature, T_s , is defined in terms of the luminosity at the surface, L_s , by

$$L_s = L_d(R) \equiv 4\pi R^2 \sigma T_s^4. \quad (10)$$

For $r \geq R$ the redshift factor is given by

$$e^{\Phi/c^2} = \left(1 - \frac{2GM}{c^2 r}\right)^{1/2} = e^{-\Lambda}.$$

Semiquantitative estimates (Ray 1981) and detailed calculations of neutron star evolution (Malone 1974; Nomoto and Tsuruta 1981; Richardson *et al.* 1982) show that for most neutron stars more than a few tens of years old, the temperature at densities less than $\sim 10^{10} \text{ g cm}^{-3}$ has fallen below 10^9 K and is decreasing sufficiently slowly so that this low-density region is quasi-stationary, and the time derivative in equation (8) can be neglected. In our model calculations of neutron star envelopes (see § IV), we have set the envelope-core boundary at a density of $10^{10} \text{ g cm}^{-3}$ (this value was also used by Glen and Sutherland 1980 in their model calculation of neutron star cooling, and Van Riper and Lamb's 1981 boundary temperature is estimated at densities close to this). We find that to a good degree of approximation the temperature has leveled off to a constant value by this density except for the hottest envelopes considered in our calculations (see Fig. 5 and § IV below).

In what follows we will denote surface values by the subscript s and inner boundary values (i.e., quantities evaluated at the envelope-core boundary) by the subscript b . When making numerical estimates, we put $\rho_b = 10^{10} \text{ g cm}^{-3}$, and the corresponding pressure is $P_b = P(\rho_b) \approx 7.3 \times 10^{27} \text{ dyn cm}^{-2}$. We shall also use the notation $Y_n = Y/10^n[Y]$, where n is an integer, and $[Y]$ stands for the units of the quantity Y . We use cgs units, and K for the temperature. Thus, for example, $g_{s14} = g_s/10^{14} \text{ cm s}^{-2}$.

In the envelope one can to a very good degree of approximation neglect the pressure terms in equations (4) and (6), replace the relativistic factors e^Λ and e^{Φ/c^2} by their surface values, and put m equal to the total mass of the star, M . To see this we notice first of all that $P/\rho c^2 \leq P_b/\rho_b c^2 \approx 8 \times 10^{-4}$. Furthermore, we have that $4\pi r^3 P/c^2 \leq 4\pi r^3 P_b/c^2 \lesssim 4 \times 10^{-7} (r/20 \text{ km})^3 M_\odot$, which is negligible compared with the gravitational mass of the neutron star, which is typically of order $1 M_\odot$. Hence, the TOV equation can be written as

$$\frac{dP}{dr} = -\rho \frac{Gm}{r^2} e^{2\Lambda} \quad (11)$$

in the envelope. By use of this equation, the mass equation (9), and the expression for e^Λ , equation (3), we find

$$\frac{d\Lambda}{dP} = \frac{Gm}{c^2 r^2} e^{2\Lambda} \left[\frac{r}{m} \frac{dm}{dP} - \left(\frac{dP}{dr} \right)^{-1} \right] = \frac{(1 - 3\rho/\bar{\rho})}{\rho c^2}, \quad (12)$$

where $\bar{\rho} = m/[(4\pi/3)r^3]$. Since $\bar{\rho} \sim$ central density of the star $\sim 10^{14} - 10^{15} \text{ g cm}^{-3}$, and $\rho \leq 10^{10} \text{ g cm}^{-3}$ in the envelope, we have to a very good approximation that

$$\Delta\Lambda \equiv \Lambda_b - \Lambda_s = \int_{P_s}^{P_b} \frac{dP}{\rho c^2}, \quad (13)$$

independent of the mass and radius of the star. Since most of the contribution to this integral comes from the higher density range where it is appropriate to use the equation of state for relativistic, degenerate matter, $P \propto \rho^{4/3}$, we can estimate the variation of Λ through the envelope by

$$\begin{aligned} \Delta\Lambda &\approx 4 \left(\frac{P_b}{\rho_b c^2} \right) \left[1 - \left(\frac{\rho_s}{\rho_b} \right)^{1/3} \right] \\ &\lesssim 4 \left(\frac{P_b}{\rho_b c^2} \right) \approx 3.2 \times 10^{-3}. \end{aligned}$$

Hence,

$$\frac{e^{\Lambda_s}}{e^{\Lambda_b}} = e^{-\Delta\Lambda} \approx 1 - \Delta\Lambda \approx 1 - 4 \left(\frac{P_b}{\rho_b c^2} \right), \quad (14)$$

which shows that e^Λ is constant in the envelope to better than 0.5%. The mass of the envelope can also be estimated in a simple way. Setting $e^\Lambda = e^{\Lambda_s}$ in the TOV equation and using equation (9), we can write

$$d \left(\frac{m}{M} \right)^2 = - \frac{8\pi G}{g_s^2} \left(\frac{r}{R} \right)^4 dP \leq - \frac{8\pi G}{g_s^2} dP. \quad (15)$$

By integrating the above expression, we find for the mass of the envelope, ΔM ,

$$\frac{\Delta M}{M} \leq 1 - \left(1 - \frac{8\pi G}{g_s^2} P_b \right)^{1/2} \approx \frac{4\pi G}{g_s^2} P_b \approx \frac{6 \times 10^{-7}}{g_{s14}^2}.$$

Since $g_{s14} > 0.1$ for all neutron stars of astrophysical interest (see, e.g., Fig. 3), we can neglect the mass of the envelope and set $m = M$ in equations (4) and (6). Integration of equation (6) gives the variation of Φ through the envelope:

$$\begin{aligned} \Delta\Phi &= \Phi_b - \Phi_s = GM e^{2\Lambda_s} \int_R^{r_b} \frac{dr}{r^2} \\ &= - \int_{P_s}^{P_b} \frac{dP}{\rho} = c^2 (\Lambda_s - \Lambda_b) \end{aligned}$$

(see eq. [13]). Hence, we may put $e^{\Phi/c^2} = e^{\Phi_s/c^2} = e^{-\Lambda_s}$, and the energy transport equation (eq. [5]) can be written as

$$\frac{dT}{dr} = - \frac{3}{16\sigma} \frac{\kappa \rho}{T^3} \frac{L_d}{4\pi r^2} e^{\Lambda_s}. \quad (16)$$

Combining equations (16) and (11), we obtain the thermal structure equation for neutron star envelopes:

$$\frac{dT}{dP} = \frac{3}{16\sigma} \frac{\kappa}{T^3 g_s} \frac{L_d}{4\pi R^2}. \quad (17)$$

The largest errors made in deriving this result are of order $4(P_b/\rho_b c^2) \approx 3.2 \times 10^{-3}$, independent of the mass and radius of the star.

When the envelope is in a quasi-stationary state (see the discussion above) and neutrino losses within the envelope can be neglected, the factors $c_v(dT/dt)$ and ϵ_v in equations (8) and (7), respectively, can be neglected, and $Le^{2\Phi/c^2}$ and $L_v e^{2\Phi/c^2}$ are constant through the envelope. Since e^{Φ/c^2} is essentially constant in the envelope, we may put $L_d (= L - L_v)$ equal to its surface value $L_s = 4\pi R^2 \sigma T_s^4$, and equation (17) can be written as

$$\frac{dT}{dP} = \frac{3}{16} \frac{\kappa}{T^3} \frac{T_s^4}{g_s}.$$

This is our thermal structure equation (eq. [1]). We note that equation (1) is just what one would obtain from a plane-parallel approximation, but we have not made this approximation.

Putting L_d equal to a constant requires that the variation of L_d through the envelope, $\Delta L_d = L_s - L_b$, where $L_b = L_d(\rho_b)$, be small compared with the surface luminosity, i.e.,

$$\left| \frac{\Delta L_d}{L_s} \right| \ll 1. \quad (18)$$

By use of equations (7), (8), and (11), we find

$$\left| \frac{\Delta L_d}{L_s} \right| = \frac{1}{\sigma T_s^4 g_s} \left| \int_{P_s}^{P_b} \left[c_v \left(\frac{T}{t_{\text{cool}}} \right) e^{-\Phi_s/c^2} - \epsilon_v \right] \left(\frac{r}{R} \right)^4 \frac{dP}{\rho} \right|, \quad (19)$$

where we have introduced the cooling time defined by

$$t_{\text{cool}}(T) = -T \left/ \left(\frac{dT}{dt} \right) \right. . \quad (20)$$

We can get a rough estimate of the values of t_{cool} for which condition (18) is satisfied. Most of the contribution to the integral in equation (19) comes from the high-density envelope layers. Hence, we assume that $P \propto \rho^{4/3}$. To find the maximum effect of the specific heat term we put the specific heat equal to that of a Dulong-Petit solid and a degenerate relativistic electron gas:

$$c_v = 3n_i k + \pi^2 k n_e \frac{kT}{\epsilon_F} \\ \approx (4.5 \times 10^{16} \rho_{10} + 3.9 \times 10^{16} \rho_{10}^{2/3} T_9) \text{ ergs cm}^{-3} \text{ K}^{-1}.$$

Here k is the Boltzmann constant, ϵ_F is the Fermi energy of the electrons, and n_e and n_i are the number densities of electrons and ions, respectively. The neutrino

emissivity is dominated by neutrino pair bremsstrahlung, whose emissivity is given by (Soyeur and Brown 1979)

$$\epsilon_v \approx 6 \times 10^{19} \left(\frac{\rho}{\rho_0} \right) T_9^6 \text{ ergs s}^{-1} \text{ cm}^{-3} \\ = 2 \times 10^{15} \rho_{10} T_9^6 \text{ ergs s}^{-1} \text{ cm}^{-3},$$

where $\rho_0 = 2.8 \times 10^{14} \text{ g cm}^{-3}$ is the density of nuclear matter. To estimate the temperature range for which variations of L_d within the envelope are unimportant, we approximate the temperature by a constant equal to $T_b = T(\rho_b)$ in the part of the envelope which contributes most to the integral in equation (19), and we neglect the deviations of $e^{-\Phi_s/c^2}$ and r/R from unity. We then find that condition (18) is satisfied if

$$\left| \frac{180 T_{b9} (1 + 1.2 T_{b9})}{t_{\text{cool}}(T_b)} - 0.28 T_{b9}^6 \right| \ll T_{s6}^4 g_{s14}, \quad (21)$$

where $t_{\text{cool}}(T_b)$ is in years. In our thermal structure calculations (see § IV and Gudmundsson, Pethick, and Epstein 1982), where condition (18) is assumed to hold, we find that T_b is related to T_s and g_s by

$$T_{b9} = 0.1288 \left(\frac{T_{s6}^4}{g_{s14}} \right)^{0.455}$$

for

$$10^{-2} \leq \frac{T_{s6}^4}{g_{s14}} \leq 10^2.$$

Using this relation in equation (21), we find that for $T_{b9} < 1$ the cooling time must satisfy

$$t_{\text{cool}}(T_b) \gg \frac{23 \text{ yr}}{T_{s6}^{2.18} g_{s14}^{1.46}} \approx \frac{2 \text{ yr}}{T_{b9}^{1.2} g_{s14}^2}. \quad (22)$$

We note that $t_{\text{cool}}(T_b)$ depends primarily on the heat content of the core and the total emissivity, which is mainly due to neutrino losses from the core during the first 10^4 – 10^5 yr. From equation (22) we see that condition (18) is most severe for very rapid cooling, which would occur if a pion condensate or free quarks were present in neutron star interiors.

It may sometimes be of interest to determine P and T as functions of depth in the envelope. For this purpose it is convenient to introduce a depth coordinate z , which is related to r and the depth coordinate $x = R - r$ by

$$z = - \int_R^r \left(\frac{R}{r'} \right)^2 e^{\Lambda_s} dr' = \int_0^x \left(\frac{R}{R-x'} \right)^2 e^{\Lambda_s} dx'. \quad (23)$$

The above expression may be integrated to give

$$x = z e^{-\Lambda_s} \left(1 + \frac{z e^{-\Lambda_s}}{R} \right)^{-1}$$

or

$$z = x e^{\Lambda_s} \left(1 - \frac{x}{R} \right)^{-1}. \quad (24)$$

In terms of this new coordinate, the TOV equation (eq. [11]) and the energy transport equation (eq. [16]) take the forms

$$\frac{dP}{dz} = \rho g_s, \quad (25)$$

and

$$\frac{dT}{dz} = \frac{3}{16} \frac{\kappa \rho}{T^3} T_s^4, \quad (26)$$

where we have assumed condition (18) by setting $L_d = 4\pi R^2 \sigma T_s^4$ in equation (16). Using equation (25), the thickness of the envelope can easily be estimated by evaluating z_b ,

$$z_b = \int_0^{z_b} dz = \frac{1}{g_s} \int_{P_s}^{P_b} \frac{dP}{\rho} \approx \frac{4}{g_s} \left(\frac{P_b}{\rho_b} \right) \approx \frac{0.3 \text{ km}}{g_{s14}}. \quad (27)$$

We have assumed $P \propto \rho^{4/3}$ when performing the integration. We stress that the largest terms neglected in equations (25) and (26) are of order $\sim 0.5\%$. We have not neglected terms of order x_b/R , which can be as large as 10% . We note, however, that if one is willing to accept errors of this order, when calculating T and P as functions of x , one can replace z by $x e^{\Lambda_s}$ in equations (25) and (26).

Given the opacity and the equation of state one can integrate equation (1) (or eqs. [25] and [26]) inward from the surface of the star. In § IV we shall present the results of our model calculations of neutron star envelopes. The input physics used in our calculations is discussed in the next section.

III. THE PHYSICAL INPUT

In this section we discuss the basic physical conditions in the matter in neutron star envelopes when there is no magnetic field present (for a more detailed discussion see Gudmundsson 1981). For astrophysically interesting models we need the physics of matter in the temperature range $10^5 \lesssim T \lesssim 10^9$ K and in the density range $10^{-4} \lesssim \rho \lesssim 10^{11}$ g cm $^{-3}$. Information about the basic properties of matter is summarized in Figures 1 and 2, and to indicate which regions are of interest, we also show temperature-density profiles for neutron star envelopes for surface temperatures of $10^{5.5}$, 10^6 , and $10^{6.5}$ K and a surface gravity of 10^{14} cm s $^{-2}$.

The equation of state has been worked on extensively. (See, e.g., Cox and Giuli 1968; Clayton 1968; Huebner *et al.* 1977. The last reference describes the numerical calculations of the Los Alamos group, and we shall refer to it in what follows as LA). However, since the physics is relatively straightforward in the regions of interest to us here, we shall not take over directly the earlier work but rather construct a simplified equation of state which is adequate for our purposes. Our equation of state agrees well with the earlier work in their regions of common validity.

Throughout most of the region of interest for our investigation, we are dealing with a finite-temperature ionized plasma. As a good first approximation one can treat matter as a two-component plasma with one species, the ions (consisting of nuclei and some bound electrons), immersed in a uniform neutralizing background of free electrons. No other particles (except photons) are

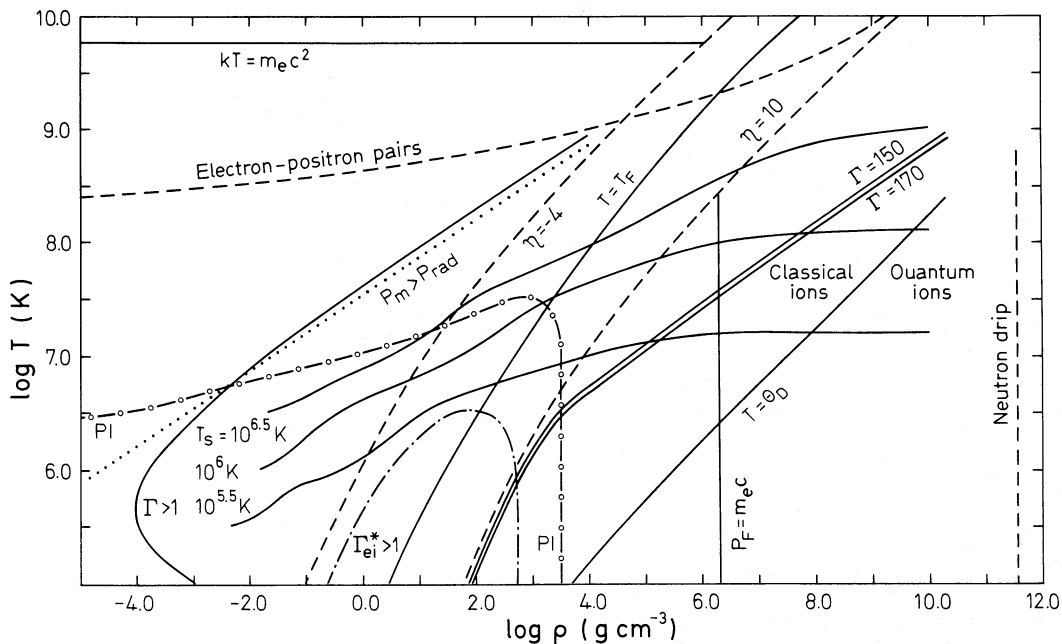


FIG. 1.—Physical conditions at densities and temperatures of interest in the study of neutron star envelopes. The various regions are identified in the text. Also shown are temperature-density profiles for envelopes for three values of the surface temperature and a surface gravity of 10^{14} cm s $^{-2}$.

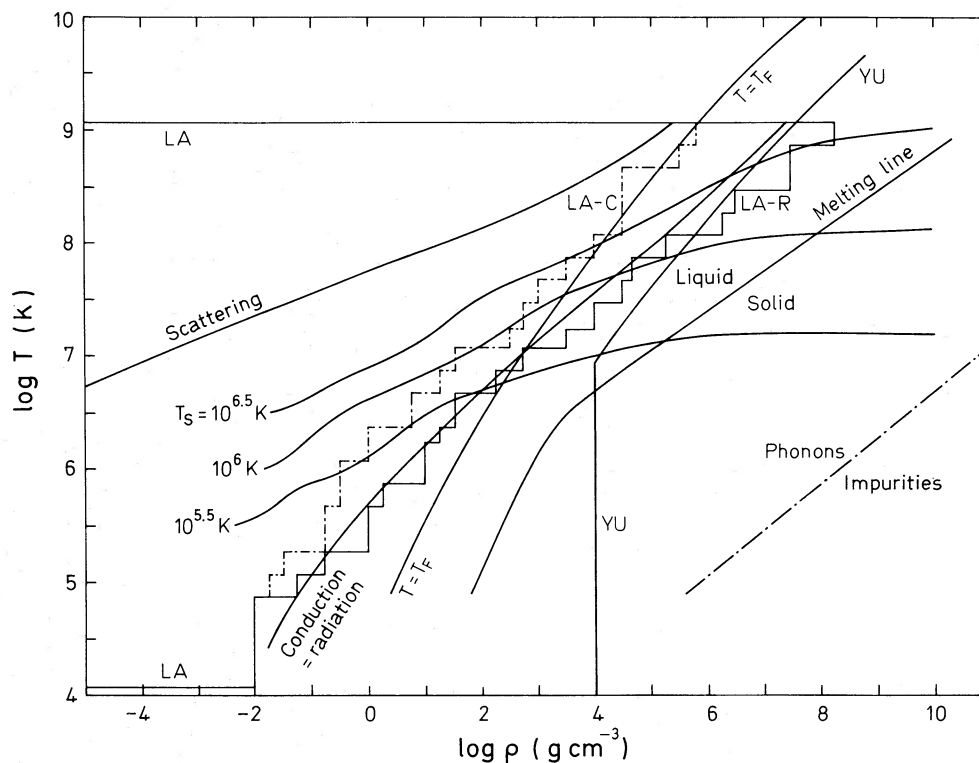


FIG. 2.—The dominant sources of opacity at various densities and temperatures. Also shown are temperature-density profiles for neutron star envelopes for three values of the surface temperature and a surface gravity of 10^{14} cm s^{-2} . See text for further explanations.

present. For example, free neutrons do not appear until the “neutron drip” density, $\rho \approx 4.3 \times 10^{11}$ g cm^{-3} , well beyond our envelope-core boundary (which we have set at $\rho = 10^{10}$ g cm^{-3}). The neutron drip point is indicated by a vertical dashed line in Figure 1. Furthermore, radiation pressure is less than the pressure of the matter below the dotted line in Figure 1.

We begin by discussing the general properties of the free-electron gas and the ions and then go on to describe the equation of state and the opacity used in our model calculations.

The free electrons in neutron star envelopes can exhibit all degrees of degeneracy. This can be seen from Figure 1, where we show the Fermi temperature T_F , as a function of density as well as the region of partial degeneracy, which is approximately bounded by the two dashed lines marked $\eta = -4$ and $\eta = 10$, where $\eta = \mu/kT$ is the degeneracy parameter, and μ is the electron chemical potential. The Fermi temperature is given by $T_F = (\epsilon_F - m_e c^2)/k$, where $\epsilon_F = (m_e^2 c^4 + p_F^2 c^2)^{1/2}$ is the Fermi energy, $p_F = \hbar(3\pi^2 n_e)^{1/3} \approx 1.009(\rho_6/\mu_e)^{1/3} m_e c$ is the Fermi momentum, and m_e and \hbar are the electron rest mass and Planck’s constant, respectively. Hence, the Fermi temperature can be written in terms of the density as

$$T_F \approx 6 \times 10^9 (\rho_6/\mu_e)^{2/3} \{1 + [1 + (\rho_6/\mu_e)^{2/3}]^{1/2}\}^{-1} \text{ K} .$$

The quantity $\mu_e = A/\langle Z \rangle$ is the mean molecular weight

per electron, where A is the mass number of the ions, and $\langle Z \rangle$ is their effective charge, which depends on the charge of the nucleus, Z , and the number of bound electrons.

In our calculations we have generally assumed that the nucleus present is that for cold catalyzed matter at the same density, and we have used the sequence of nuclei determined by Baym, Pethick, and Sutherland (1971). For densities less than 6.6×10^6 g cm^{-3} the nucleus present is ^{56}Fe . In the region where the nuclei are partially ionized we have used the Los Alamos numerical determination of $\langle Z \rangle$ for ^{56}Fe (LA) as well as the numerical calculations of Malone (1974), which extend to slightly higher densities than those of LA. The line marked PI in Figure 1 shows approximately the boundary of the region of partial ionization.

Since the temperature in the neutron star envelopes of interest to us here is much less than $(m_e c^2)/k \approx 5.93 \times 10^9$ K, nondegenerate electrons are non-relativistic. Furthermore, we do not have to consider electron-positron pairs; their presence can be neglected below the dashed line near the top in Figure 1. (See, e.g., Cox and Giuli 1968 for determination of the region where electron-positron pairs exist in nonnegligible numbers.) It is only when $p_F \gtrsim m_e c$, i.e., for densities in excess of $\sim 2 \times 10^6$ g cm^{-3} , that degenerate electrons are relativistic.

The electrons not bound to ions can be affected by

Coulomb interactions both with other electrons and with ions. The perturbative effects of the ions are $\sim \langle Z \rangle^{2/3}$ times those of the electrons, so the electron-ion interaction is the more important one. In general, one can define a dimensionless measure of this coupling by $\Gamma_{ei}^* \equiv \langle Z \rangle e^2 / (r_i k T^*)$, where $r_i = [(4\pi/3)n_i]^{-1/3}$ is the radius of the Wigner-Seitz sphere, e is the charge of the electron, and $k T^*$ is a measure of the kinetic energy of the electron gas. We shall take $k T^* = P_e / n_e$, where P_e is the pressure of an ideal electron gas, and therefore, $T^* = T$ for nondegenerate nonrelativistic electrons, $T^* = \frac{2}{3} T_F$ for degenerate nonrelativistic electrons, and $T^* = \frac{1}{4} T_F$ for degenerate relativistic electrons. When $\Gamma_{ei}^* \gg 1$, the electron density will deviate appreciably from uniformity, and the ideal gas approximation is no longer valid. In Figure 1 the region bounded by the dot-dashed contour has $\Gamma_{ei}^* > 1$. We see that for neutron star envelopes with surface temperatures $\gtrsim 3 \times 10^5$ K, the unbound electrons can to a good degree of approximation be taken to be an ideal gas everywhere.

In marked contrast to the free electrons, the ions in neutron star envelopes are strongly affected by Coulomb perturbations even at relatively low densities and high temperatures. The ion thermal velocities are only of order $\sim (kT/Am_H)^{1/2} \approx 3.9 \times 10^7 (56/A)^{1/2} T_9^{1/2}$ cm s $^{-1}$, where m_H is the atomic mass unit. The ions are therefore nonrelativistic throughout the envelope, and the effects of the ion-ion Coulomb interaction, which are characterized by the dimensionless parameter $\Gamma = (\langle Z \rangle^2 e^2 / r_i k T) \approx 0.87 / T_7 (\langle Z \rangle / 26)^2 (56/A)^{1/2} \rho_{-2}^{1/2}$, are important even at the surface of the neutron star. In Figure 1 we show the contour for $\Gamma = 1$. To the right of this contour, Γ is greater than 1. The value of Γ increases with density, and at a critical melting value, Γ_m , a liquid-solid transition takes place; above $\Gamma = \Gamma_m$, the ions form a solid. The melting temperature of the solid can be written in terms of Γ_m as $T_m \approx 1.44 \times 10^3 \langle Z \rangle^{5/3} (\rho/\mu_e)^{1/3} (158/\Gamma_m)$ K, where we have normalized Γ_m in terms of the characteristic value 158 (Pollock and Hansen 1973) used in our numerical calculations. There is some uncertainty in the actual value of Γ_m . For example, Pollock and Hansen (1973) using another method found $\Gamma_m = 155 \pm 10$, and the most recent determination gives $\Gamma_m = 171 \pm 3$ (Slattery, Doolen, and DeWitt 1980). In Figure 1 we have drawn lines for both $\Gamma = 150$ and $\Gamma = 170$ to indicate the uncertainty in Γ_m . However, the results of our calculations are not very sensitive to Γ_m (see § VII).

Figure 1 also shows the Debye temperature, θ_D , as a function of density. For ions arranged in a bcc lattice, θ_D is given by $\theta_D \approx 0.45 \hbar \Omega_p / k$, where $\Omega_p = [4\pi \langle Z \rangle^2 e^2 \times (n_i/m_i)]^{1/2}$ is the ion plasma frequency, and m_i is the mass of the ions (Carr 1961). We see that $T < \theta_D$ only at the highest densities and lowest temperatures occurring in neutron star envelopes. Since the contribution of the ions to the total pressure in this region is small, we can for the purpose of thermal structure calculations neglect quantum effects in the equation of state and treat the ions as classical everywhere.

The effects of the Coulomb interaction on the ion equation of state can be taken into account by adding correction terms to the ideal gas law $P_{\text{ion}} = n_i k T$ (see, e.g., Salpeter 1961; Shaviv and Kovetz 1972; and references therein). For the conditions of interest the corrections are dominated by the classical Coulomb correction, which takes into account the electrostatic shielding of ions by the mean charge density of the electrons, and we therefore ignore other effects (such as the Thomas-Fermi and the exchange corrections) in our equation of state. Denoting the pressure correction term by P_c , we can write $P_c = \frac{1}{3} (U_c / k T) P_{\text{ion}}$, where U_c is the Coulomb excess internal energy per ion. (Note that U_c is negative.) For $U_c / k T$ we use the results of the Monte Carlo calculations of Hansen (1973) and Pollock and Hansen (1973).

The radiation pressure in the envelopes of interest can be neglected, and our equation of state is therefore given by

$$P = P_e(n_e, T) + n_i k T + \frac{1}{3} n_i U_c, \quad (28)$$

where $P_e(n_e, T)$ is the pressure of the free electrons, which are treated as an ideal Fermi gas, and $n_e = \langle Z \rangle n_i$. The quantity $P_e(n_e, T)$ is calculated by an approximation scheme devised by Eggleton, Faulkner, and Flannery (1973) which approximates the Fermi-Dirac integrals for the density and pressure to a few parts in a thousand.

We now discuss the opacity used in our calculations. The thermal energy transport in neutron star envelopes takes place by a combination of radiative diffusion and thermal conduction. The total opacity, κ , is given by

$$\frac{1}{\kappa} = \frac{1}{\kappa_{\text{rad}}} + \frac{1}{\kappa_{\text{cond}}}, \quad (29)$$

where κ_{rad} is the Rosseland mean radiative opacity, and κ_{cond} is the conductive opacity, which is related to the net thermal conductivity λ_c by $\kappa_{\text{cond}} = 16\sigma T^3 / (3\rho\lambda_c)$. The radiative opacity has contributions from bound-bound, bound-free, and free-free absorptions of photons as well as from Thomson scattering of photons by free electrons. The main scattering processes which contribute to κ_{cond} are electron-phonon, electron-impurity, and electron-electron scattering when the matter is solid, and electron-ion and electron-electron scattering when the matter is liquid.

In our calculations we used the Los Alamos radiative and conductive opacities (LA) in the regions where they are available. At higher densities we used conductive opacities calculated by Urpin and Yakovlev (1980) and Yakovlev and Urpin (1980), referred to in what follows as YU. In Figure 2 we show the regions over which we used the LA and YU opacities. Below and to the right of the line marked YU we used the YU conductive opacities. The upper part of the YU contour corresponds to $T = \frac{1}{10} T_F$. The step-line boundaries show the regions in which we used the LA radiative opacity (*solid line*) and conductive opacity (*dot-dashed line*). The regions are different because we omitted points in the conductive opacity calculated using Mestel's (1950) results which

do not join smoothly onto the other points calculated by Hubbard and Lampe (1969). For densities at which no calculations exist we used a straight-line logarithmic interpolation between the cut-off densities for the LA and YU conductive opacities at the same temperature. It was also necessary to extrapolate the radiative opacities to higher densities. The way in which this was done has very little effect on the results; for a fixed temperature we used a straight-line logarithmic extrapolation, with a slope equal to that at the last calculated points. A change of this slope by a factor of 10 typically results in a change in T_b of less than 0.5%.

Figure 2 gives information about the relative importance of the various processes which contribute to the total opacity. Below the line marked "conduction = radiation," heat transport is primarily by conduction, and above it by radiation. Above the line marked "scattering," Thomson scattering is the most important process. In between these two lines the opacity is dominated by bound-bound, bound-free, and free-free absorptions. Between the lines labeled "conduction = radiation" and "melting line," electron-ion scattering is the most important process. Between the melting line and the dot-dashed line, electron-phonon scattering is the dominant process, and below the dot-dashed line, electron-impurity scattering contributes most to the total opacity. The exact location of this line depends on the value of the impurity parameter $X_I = X_{\text{imp}} \langle \Delta Z \rangle^2$, where X_{imp} is the relative abundance of impurities, and $\langle \Delta Z \rangle^2$ denotes the average departure of Z_{imp}^2 (Z_{imp} = charge of the impurities) from Z^2 . The value of X_I is not known but is usually assumed to be of order unity, and we therefore put $X_I = 1$ in our basic thermal structure calculations. We find that the results are not very sensitive to X_I ; for $X_I < 10$ and surface temperatures $\geq 10^{5.5}$ K, a factor of 10 variation of X_I results in a less than 1% change in the calculated value of T_b .

It should also be mentioned that under all conditions of interest to us here electron-electron scattering contributes very little to the conductive opacity and can for all practical purposes be neglected.

The YU conductive opacities used in our calculations differ considerably from those calculated by Flowers and Itoh (1976) (referred to as FI in what follows), which have been used in most other recent calculations. For example, YU's results for the electron-phonon contribution to the opacity are typically some 2–5 times larger than FI's, and their results for the electron-ion contribution are typically 2–3 times larger. We used the YU results rather than those of FI for a number of reasons. First, in the case of a solid, FI's estimates for the transverse phonon frequencies are systematically too high and lead to values of the thermal conductivity that are too high. YU's results, on the other hand, are based on detailed calculations of moments of the phonon spectrum for the Coulomb lattice. Second, for the liquid phase the YU calculations are in better agreement with estimates made by Nandkumar and Pethick (1982), who used improved results for the structure factor of the one-component plasma, than are those of FI.

IV. CALCULATIONS

The surface temperature, T_s , and the surface gravity, g_s , specify the thermal structure of a neutron star envelope. We therefore start this section by discussing the relevant ranges of these quantities.

The recent X-ray observations by the *Einstein Observatory* have given several upper limits to the X-ray luminosities of neutron stars possibly present in young supernova remnants (Cas A [Murray *et al.* 1979]; Kepler, RCW 86, W28, G350.0–18, G22.7–0.2 [Helfand, Chanan, and Novick 1980]; SN 1006 [Pye *et al.* 1981]; Tycho [Gorenstein and Seward, quoted, e.g., by Van Riper and Lamb 1981]) and three detections (the Crab and Vela pulsars [Harnden *et al.* 1979a, b] and RCW 103 [Tuohy and Garmire 1980]). In addition, upper limits have been obtained for seven nearby radio pulsars (Helfand, Chanan, and Novick 1980). The surface temperatures of the neutron stars (or the upper limits) deduced from the flux measurements are somewhat uncertain, mainly because of uncertainty in the interstellar absorption. With the uncertainties taken into account, the upper limits on the surface temperatures of neutron stars lie between

$$2 \times 10^5 \lesssim T_{s, \text{upper limit}} \lesssim 3 \times 10^6 \text{ K}, \quad (30)$$

the highest value, 3×10^6 K, corresponding to the upper limit to the surface temperature of the Crab pulsar. Surface emission from neutron stars with $T_s \lesssim 2 \times 10^5$ K is probably too weak to be observed in

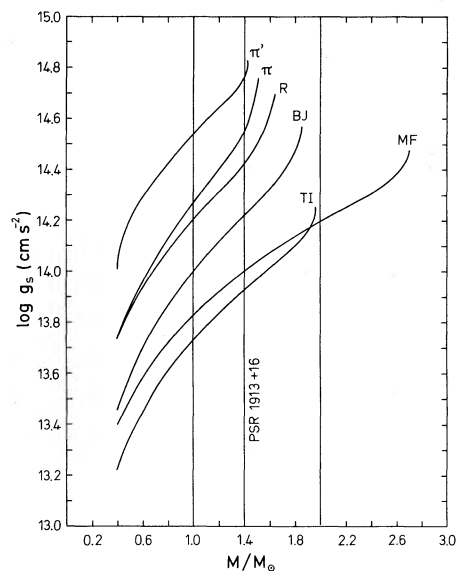


FIG. 3.—The surface gravity of neutron stars as a function of gravitational mass for neutron star models calculated with several equations of state. The masses and radii needed to calculate the surface gravities were taken from Baym and Pethick (1979), and we also use their notation for the different equations of state. MF is the Pandharipande–Smith (1975b) mean field theory calculation, TI is their tensor interaction model calculation (Pandharipande and Smith 1975a), BJ denotes the Bethe–Johnson (1974) equation of state I, R denotes the pure neutron equation of state with the Reid potential (Pandharipande 1971), and π and π' denote equations of state for matter with pion condensates present (Maxwell and Weise 1976).

the near future (see, e.g., Helfand, Chanan, and Novick 1980), and we therefore take equation (30) to be the range of observational interest.

Observations of neutron stars suggest that they have masses exceeding $1 M_{\odot}$. The best mass determination is for the binary radio pulsar PSR 1913+16, with $M = 1.39 \pm 0.15 M_{\odot}$ (Taylor, Fowler, and McCulloch 1979), and masses have also been obtained for a few binary X-ray pulsars. The uncertainties are larger in this case, but for the five best studied sources (4U 0900-40, SMC X-1, Cen X-3, 4U 1538-52, and Her X-1) Rappaport and Joss (1981) find that the most probable values for all the masses lie in the range $1 \leq M \leq 2 M_{\odot}$ (see also Bahcall 1978). This is consistent with the results of stellar evolutionary calculations (see, e.g., Weaver, Zimmerman, and Woosley 1978) which predict neutron star masses of order $1.5 M_{\odot}$. In Figure 3 we show the surface gravity of a neutron star,

$$g_s = \frac{GM}{R^2} e^{\Lambda_s} = 1.33 \times 10^{14} \left(\frac{M}{M_{\odot}}\right) R_6^{-2} \times \left[1 - 0.295 \left(\frac{M}{M_{\odot}}\right) R_6^{-1}\right]^{-1/2} \text{ cm s}^{-2},$$

as a function of the gravitational mass, M , for neutron star models calculated with several equations of state. Since neutron stars with masses lower than $0.4 M_{\odot}$ probably do not exist (see the discussion above), and this is the lowest mass for which neutron star cooling calculations have been performed, we only show g_s for stars with $M \geq 0.4 M_{\odot}$. The vertical lines in Figure 3 correspond to masses $1.0 M_{\odot}$, $1.4 M_{\odot}$ (PSR 1913+16), and $2.0 M_{\odot}$. Under the assumptions that neutron stars have masses $M \geq 1 M_{\odot}$ and that the equations of state of Figure 3 bound the correct equation of state, Figure 3 gives the limits on the range of astrophysically relevant neutron star surface gravities to be

$$10^{13.7} \lesssim g_s \lesssim 10^{14.9} \text{ cm s}^{-2}. \quad (31)$$

The box in Figure 4 shows the area in the (g_s, T_s) parameter space which lies within the bounds of equations (30) and (31). The crosses show the (g_s, T_s) pairs used in our model calculations. For each pair the structure equations (25) and (26) were integrated inward from the surface to a density of $\rho_b = 10^{10} \text{ g cm}^{-3}$.

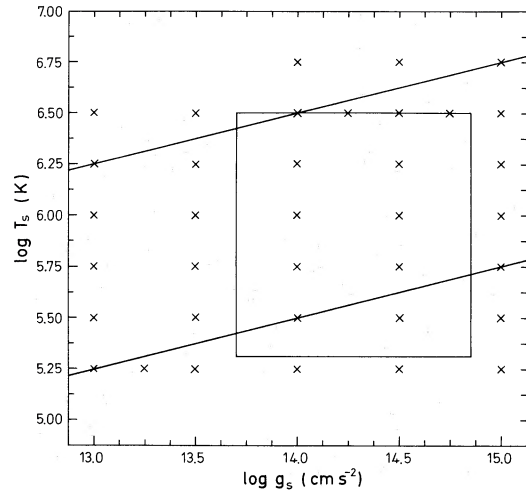


FIG. 4.—The (g_s, T_s) parameter space for neutron stars. The box encloses the area which is presently of astrophysical interest. The crosses show the (g_s, T_s) pairs used in our model calculations. The two inclined lines bound the region for which our calculations give reliable results.

The two inclined lines bound the region for which our calculations give reliable results. Above the upper line, no reliable calculations of envelope opacities exist for part of the required range of temperatures and densities, and below the lower line, the temperature profiles pass through the region where $\Gamma_{ei}^* > 1$, and our equation of state and opacities are unreliable.

The boundary temperature, T_b , as a function of T_s and g_s is shown in Table 1. The first thing to notice is that to better than about 1 part in 10^4 , T_b is a function only of T_s^4/g_s . The reason for this can be seen by an inspection of the structure equation (1). One can see that $T = T(P)$ depends only on the combination T_s^4/g_s and the outer boundary condition. However, because of the rapid decrease of radiative opacities with increasing temperature, the solutions to equation (1) converge very rapidly to the radiative zero solution as the density increases, and hence, the surface condition plays a very small role in determining the interior temperature profile. This convergence is illustrated in Figure 5, where pairs of temperature profiles with the same values of T_s^4/g_s but different surface temperatures rapidly approach

TABLE 1
VALUES OF LOG T_b AS A FUNCTION OF LOG T_s AND LOG g_s

log T_s	log g_s				
	13.0	13.5	14.0	14.5	15.0
5.25	7.19805	6.96627
5.50	7.65854	7.42932	7.19800	6.96628	...
5.75	8.10995	7.88341	7.65853	7.42930	7.19805
6.00	8.56554	8.33690	8.10995	7.88341	7.65853
6.25	9.02078	8.79672	8.56557	8.33692	8.10995
6.50	9.02073	8.79664	8.56553
6.75	9.02065

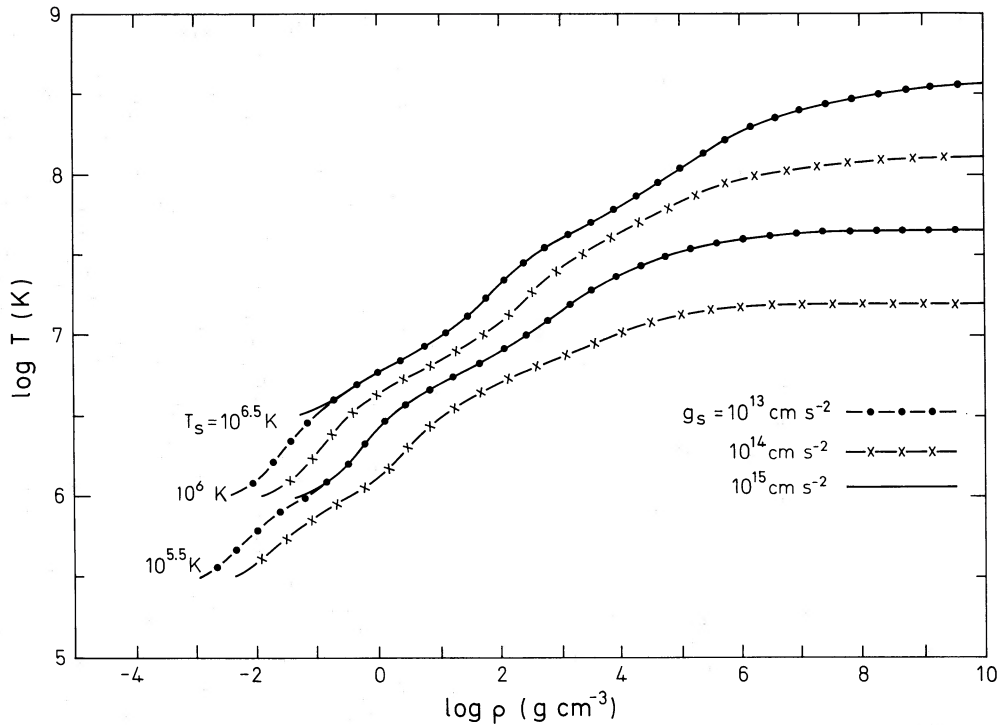


FIG. 5.—Temperature-density profiles for various values of surface temperatures and surface gravities

each other below the photospheres. This behavior is well known in the case of ordinary stellar atmospheres (see, e.g., Schwarzschild 1958).

Our results for the boundary temperature at $10^{10} \text{ g cm}^{-3}$ are accurately fitted by the expression

$$T_{b8} = 1.288(T_{s6}^4/g_{s14})^{0.455}. \quad (32)$$

This relation holds to better than 1.5% for $10^{-2} \leq T_{s6}^4/g_{s14} \leq 10^2$, or, equivalently, for $1.6 \times 10^7 \leq T_b \leq 10^9 \text{ K}$.

As mentioned in § II the redshifted temperature is nearly constant for densities above $10^{10} \text{ g cm}^{-3}$. The actual increase in Te^{0/c^2} between $\rho = 10^{10} \text{ g cm}^{-3}$ and $10^{11} \text{ g cm}^{-3}$ is found from our calculations to be approximately a factor of $[1 + 9.7 \times 10^{-3}(T_{s6}^4/g_{s14})^{0.50}]$. This increase is less than 1% for $T_s/g_{s14}^{1/4} \lesssim 10^6 \text{ K}$ and is $\sim 3\%$ and $\sim 10\%$ for $T_s/g_{s14}^{1/4} = 10^{6.25} \text{ K}$ and $10^{6.50} \text{ K}$, respectively.

In the above calculations it was found that the depth coordinate at the inner boundary at $10^{10} \text{ g cm}^{-3}$ is

$$z_b = \frac{0.310}{g_{s14}} \text{ km}, \quad (33)$$

in good agreement with estimates presented in § II (see eq. [27]). Note that the depth coordinate and the radial coordinate are related by equation (24), and that the variation of z with density near the boundary goes roughly as $\rho^{1/3}$ (for example, our calculations give $z[\rho = 10^{11} \text{ g cm}^{-3}] = 2.03z[\rho = 10^{10} \text{ g cm}^{-3}]$). Figures 5 and 6 shows runs of temperatures with density and

depth, respectively, for three surface temperatures and a range of surface gravities.

V. SCALING RELATIONS

Because T_b depends only on T_s^4/g_s , it is possible to derive a number of scaling relations. By inverting this relationship, we obtain

$$T_s^4 = g_s f(T_b), \quad (34)$$

where f is some function which depends only on T_b , the opacity, and the equation of state. Using

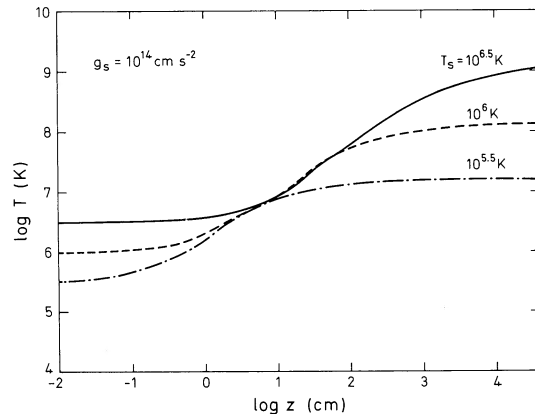


FIG. 6.—Temperature as a function of depth for three surface temperatures and a surface gravity of $10^{14} \text{ cm s}^{-2}$.

equation (2) for g_s and the fact that $e^{\Lambda_s} = e^{-\Phi_s/c^2}$ in the envelope, we can express the surface luminosity as

$$L_s = 4\pi R^2 \sigma T_s^4 = e^{-\Phi_s/c^2} 4\pi \sigma G M f(T_b). \quad (35)$$

The luminosity far from the star is given by

$$L_\infty = L_s e^{2\Phi_s/c^2} = 5.4 \times 10^{32} \left(\frac{M}{M_\odot}\right) T_{b8}^{2.2} \times \left[1 - 0.295 \left(\frac{M}{M_\odot}\right) R_6^{-1}\right]^{1/2} \text{ ergs s}^{-1}, \quad (36)$$

where the numerical expression is obtained by use of our $T_b - T_s$ relation, equation (32). Since the R^2 factor in the surface area is canceled by the $1/R^2$ factor in the surface gravity, the luminosity depends almost linearly on the stellar mass and only weakly on the stellar radius, through the redshift factor. Equations (35) and (36) enable us to understand Van Riper and Lamb's (1981) observation that for a given core temperature, L_∞ is essentially independent of R for neutron star models of the same mass.

The general scaling relation, equation (34), can be used to determine the sensitivity of the thermal structure to gross variations in the input physics. For example, if the opacity is everywhere multiplied by a factor α , it is equivalent in equation (1) to multiplying the surface gravity by α^{-1} so that the flux is changed by a factor α^{-1} . Additional sensitivity tests are discussed in § VII.

VI. GENERAL RELATIVISTIC EFFECTS

General relativity plays a role in the hydrostatic structure of the envelope, in the energy transport through the envelope, and in the relation between L_∞ and L_s . To understand the interplay of these different effects we distinguish three levels of approximation in which general relativity is incorporated to varying degrees in the investigation of neutron star thermal evolution: the full treatment, in which both stellar structure and energy transport are treated relativistically, the semirelativistic approximation, in which the structure is treated rela-

tivistically but energy transport is not, and the Newtonian approximation, in which neither is treated relativistically. In many of the earlier calculations of neutron star cooling, the semirelativistic approximation was used (see, e.g., Tsuruta 1979), and it has been suggested that some of the differences between various model calculations may be due to differences in the treatment of relativistic effects.

To show clearly the differences among the envelope calculations in the three different approximations, we pick a neutron star with a given mass and radius. A comparison of equations (11) and (16) with equation (1) then shows that the thermal structure equations for the semirelativistic and Newtonian envelopes are obtained by replacing g_s in equation (1) by $g_s e^{-\Phi_s/c^2}$ and $g_s e^{\Phi_s/c^2}$, respectively, where g_s is given by equation (2). Assuming a fixed T_b and using equation (34), we then obtain the surface luminosities

$$L_{\text{semi}} = e^{-\Phi_s/c^2} L_s, \quad L_{\text{Newt}} = e^{\Phi_s/c^2} L_s, \quad (37)$$

where L_s is the surface luminosity as obtained in the relativistic calculation. The expression for L_{Newt} shows that general relativistic effects increase the stellar surface luminosity.

Observationally what is of interest is the luminosity as observed far from the star. In both the semirelativistic and Newtonian cases the luminosity far from the star is the same as the surface luminosity, whereas in the relativistic case it is decreased by a factor of $e^{2\Phi_s/c^2}$ because of redshifting. We therefore have that

$$L_\infty = e^{2\Phi_s/c^2} L_s,$$

and

$$L_{\text{semi}} = e^{-3\Phi_s/c^2} L_\infty, \quad L_{\text{Newt}} = e^{-\Phi_s/c^2} L_\infty. \quad (38)$$

Newtonian calculations are therefore in better agreement with the full relativistic treatment than the semirelativistic ones are. A few typical values of the redshift factors are given in Table 2. We see that for massive neutron stars with a soft equation of state, the

TABLE 2
RELATIVISTIC EFFECTS ON LUMINOSITIES

EOS ^a	$\frac{M}{M_\odot}$	$\frac{R}{\text{km}}$	$\frac{L_{\text{Newt}}}{L_\infty} = \exp\left(-\frac{\Phi_s}{c^2}\right)$	$\frac{L_{\text{semi}}}{L_\infty} = \exp\left(-\frac{3\Phi_s}{c^2}\right)$
BPS.....	0.4	10.0	1.065	1.208
	0.7	9.3	1.135	1.462
	1.25	8.13	1.35	2.46
	1.41	7.0	1.58	3.94
TI.....	0.4	17.5	1.036	1.112
	0.7	16.6	1.070	1.225
	1.25	16.0	1.14	1.48
	1.41	15.7	1.17	1.60

^a BPS denotes the Baym, Pethick, and Sutherland 1971 equation of state, which is relatively soft, whereas TI stands for the Pandharipande and Smith 1975a tensor-interaction equation of state, which is representative of the stiffer ones. Model parameters are taken from Glen and Sutherland 1980.

differences between L_{semi} and L_{∞} can be appreciable; for example, $L_{\text{semi}} = 3.94L_{\infty}$ for a $1.41 M_{\odot}$ Baym-Pethick-Sutherland (1971) star. For neutron stars with a stiff equation of state, the differences are smaller; for example, $L_{\text{semi}} = 1.60L_{\infty}$ for a $1.41 M_{\odot}$ Pandharipande-Smith (1975a) tensor interaction star.

We stress that equations (37) and (38) hold for fixed boundary temperature, T_b . There are also effects of general relativity on the behavior of T_b as a function of time, as discussed, for example, by Kindl and Straumann (1981) and Gudmundsson (1981).

VII. SENSITIVITY TESTS

In order to obtain the $T_b - T_s$ relation for neutron star envelopes one needs to know the physical input for a wide range of densities and temperatures. The equation of state is rather well understood except in the region of partial ionization; fortunately, this region is of very little importance for the range of surface temperatures we consider here. On the other hand, the opacity is uncertain in a much larger part of the ρ - T plane; in some regions no calculations exist, and in regions where there are calculations, different calculations differ by as much as a factor of 3-5 (see the discussion in § III). It is therefore important to find out at which densities and temperatures it is most crucial to know the opacity well to obtain a reliable relationship between T_b and T_s . It is clear that all regions are not equally important; for example, small errors in the opacity near the surface are quickly "forgotten" because of the rapid convergence of temperature profiles to the radiative zero solution, and small errors in the opacity near the inner boundary of the envelope are unimportant since that region is nearly isothermal. In order to find out which regions are the most important in this respect we have developed a functional derivative technique for analyzing the sensitivity of the solutions of equation (1) to uncertainties in the input physics. This technique, which can be used to determine how sensitive the solutions to any number of coupled ordinary differential equations are to variations in the input physics and boundary conditions, is described in detail by Epstein, Gudmundsson, and Pethick (1983). Here we shall only quote the results for the opacity sensitivity analysis. The change in the boundary temperature, T_b , of an envelope, with fixed T_s^4/g_s , due to small changes in the opacity, κ , is given to first order by the integral

$$\Delta \ln T_b = \int_{\ln \rho_s}^{\ln \rho_b} \left(\frac{\delta \ln T_b}{\delta \ln \kappa} \right) \Delta \ln \kappa d \ln \rho, \quad (39)$$

where we use logarithmic variables; $\Delta \ln \kappa$ is a small variation in $\ln \kappa$ at density ρ , and $\delta \ln T_b / \delta \ln \kappa$ is the functional derivative of $\ln T_b$ with respect to $\ln \kappa$ evaluated at $\ln \rho$. Note that the functional derivative will depend on whether one uses $\ln \rho$ or ρ as the integration variable in equation (39). In this section we shall always use $\ln \rho$ as the variable of integration, and we will not indicate this explicitly in our notation for the functional derivative. Figure 7 shows $\delta \ln T_b / \delta \ln \kappa$ as

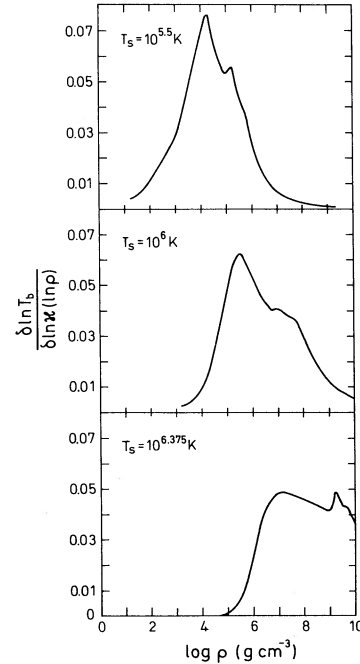


FIG. 7.—The values of the functional derivative $\delta \ln T_b / \delta \ln \kappa$ for three neutron star envelopes. The surface gravity is the same in all these cases: $10^{14} \text{ cm s}^{-2}$.

a function of density for neutron star envelopes for three values of the surface temperature and for a surface gravity of $10^{14} \text{ cm s}^{-2}$. The boundary temperature is most sensitive to variations in the opacity at densities where $\delta \ln T_b / \delta \ln \kappa$ is largest. We have defined a sensitive region in the ρ - T plane as that region for which $\delta \ln T_b / \delta \ln \kappa$ is greater than one-half of its maximum value for each envelope. This region, where it is most important to know the opacity well, is the shaded one in Figure 8. In what follows we shall refer to this region as the sensitivity strip. Almost the entire sensitivity strip is in the region where the ions are in the liquid phase and the heat transport is mainly by thermal conduction. Since the main contribution to the opacity in this region is due to electron-ion scattering, this process must be well understood to reliably evaluate the $T_b - T_s$ relation.

Heat transport by radiative diffusion plays a relatively small role in the sensitivity strip, and hence, it is reasonable that our results are not sensitive to the way in which the radiative opacity is extrapolated beyond the published LA results. However, we note that a part of the region in which one needs to interpolate between the various published calculations for the conductive opacity lies in the sensitivity strip.

The relative insensitivity of results to the radiative opacity is further demonstrated by the fact that if the total opacity is changed by a factor of 2, the boundary temperature increases by about 37% (for fixed T_s), whereas if only the radiative opacity is changed by a factor of 2, and the conductive one remains unaltered, the boundary temperature increases by less than 3%.

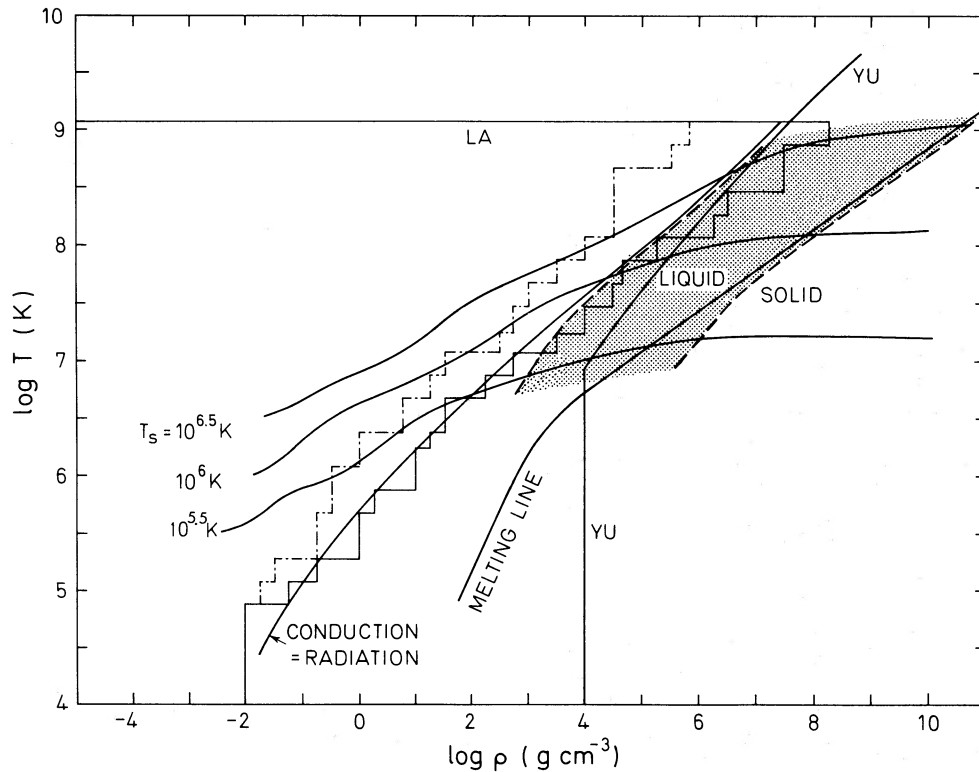


FIG. 8.—The sensitivity strip, where it is most important to know the opacity well, is indicated by the shaded area. Also shown are temperature-density profiles for $g_s = 10^{14}$ cm s $^{-2}$ and three different surface temperatures. Further explanations are in the text; also see Fig. 2.

In § III we mentioned that the YU results for the electron-ion contribution to the conductive opacity are typically 2–3 times larger than those obtained by FI. In order to see how the differences between the YU and FI results are reflected in the $T_b - T_s$ relation we have calculated a number of envelope models using the FI opacities and compared those with our YU calculations. We used the FI opacities in exactly the same regions as the YU ones before and interpolated between the FI opacities and the LA opacities in the same way (see the discussion in § III). For a given boundary temperature the luminosities of the FI envelopes are about 2–2.5 times the values for the YU envelopes (see Fig. 9). This is consistent with the luminosity-opacity scaling relation discussed in § V and the fact that in the liquid region the YU opacities are 2–3 times the FI ones. From our calculations of $\delta \ln T_b / \delta \ln \kappa$ and the differences between the YU and FI opacities, one can use equation (39) to estimate by how much the boundary temperatures of FI envelopes should deviate from those of YU envelopes with the same values of T_s^4/g_s . We have done this and find results which agree with the actual differences obtained in the full thermal structure calculations to within 10%–15%. This is a very good agreement since equation (39) is only a linear approximation.

Finally, we mention that our results are not very sensitive to variations in Γ_m , the melting value of Γ , even though the melting line lies inside the sensitivity strip. This is because the melting line lies very close to the edge of the strip, where the sensitivity is relatively low, and in addition, the difference between the thermal conductivities of the liquid and solid is small. We find that the results for the boundary temperature obtained by using $\Gamma_m = 100$ and 200 differ by less than 2% from those obtained with $\Gamma_m = 158$, the value used in all our basic calculations.

VIII. COMPARISON WITH OTHER CALCULATIONS

Even though different workers have generally made calculations for stellar models with different values of M and R , the scaling relation, equation (34), allows their results to be directly compared: T_b is mainly a function only of T_s^4/g_s and virtually independent of other aspects of the stellar structure. In fact, we may equivalently investigate the relationship between T_b and $T_s/g_s^{1/4}$, which is more convenient since it corresponds closely to what most workers have looked at in the past, namely, the relationship between T_b and T_s . Figure 9 shows $T_s/g_s^{1/4}$ and $e^{-\Phi_s} L_\infty / (M/M_\odot)$ as functions of T_b for our YU and FI model calculations and the envelope calculations of various other workers. We see

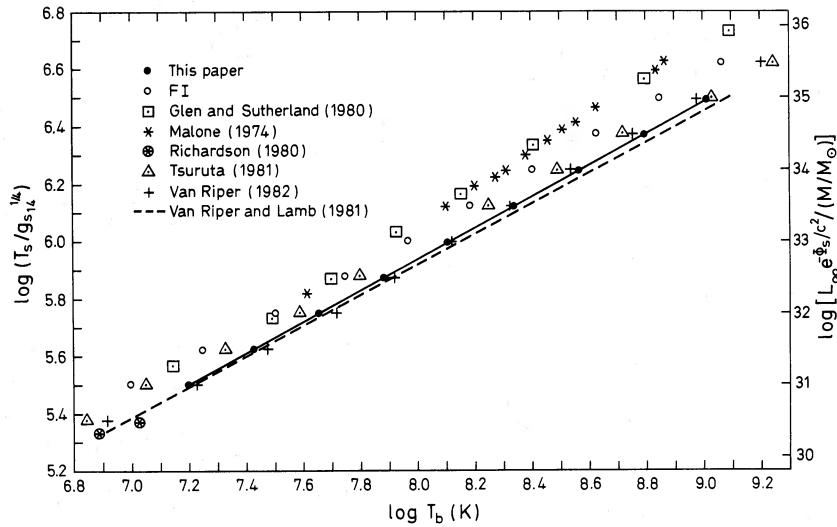


FIG. 9.—The quantities $T_s/g_{s,14}^{1/4}$ and $L_{\infty} \exp(-\Phi_s/c^2)/(M/M_{\odot})$ as functions of T_b . The open circles are results we obtained using the FI opacities instead of the YU ones. The Malone (1974) and Richardson (1980) points were taken from Richardson *et al.* (1982), where models I, II, and III correspond to Malone's calculations, and model IV and V to Richardson's. The tables in Richardson *et al.* (1982) give values of T_s and T_c , the central temperature of the neutron star models, at various times. We only used results for times ≥ 100 yr and converted central temperatures to boundary temperatures by use of the relation $T_b \exp(\Phi_s/c^2) = T_c \exp(\Phi_c/c^2)$.

that there are considerable differences among some of the results. These differences are, to a large extent, due to the use of different opacity functions in the sensitivity strip.

We first remark that the Malone points were obtained for a number of neutron star models all with different masses and different surface gravities. The fact that these points can be fitted by a smooth curve confirms our basic T_b versus $T_s/g_s^{1/4}$ scaling relation. Similar remarks apply to the Tsuruta points and to the Glen and Sutherland ones. A second point is that Figure 9 shows that luminosities we calculated using YU opacities, which we regard as the best available, lie below nearly all the other results, in some cases by as much as one order of magnitude. This shows conclusively that differences in envelope calculations can have a significant effect on predicted X-ray luminosities. A third point is that our YU results agree closely with recent calculations by Van Riper (1982), who used opacity functions and interpolation procedures similar to ours. A fourth point is that calculations with nominally the same input physics exhibit widely disparate results. For example, Glen and Sutherland (1980), Tsuruta (1981*b*), and Van Riper and Lamb (1981) all use the Los Alamos opacities at low densities and the FI conductive opacities at higher densities. We attribute the differences among these calculations and our FI results to differences in the ways various workers interpolated and extrapolated conductive opacities in the sensitivity strip, which had not been identified when the earlier calculations were carried out. Uncertainties in the equation of state are rather small for envelopes with $T_s/g_{s,14}^{1/4} > 10^{5.5}$ K, but for lower temperature neutron stars, uncertainties in how to treat partial ionization are significant.

IX. CONCLUSIONS

This investigation shows that a separate study of neutron star envelopes gives valuable insights into calculations of neutron star cooling. It was found that the temperature at the inner boundary of the envelope, T_b , is a universal function of the single parameter $T_s/g_s^{1/4}$ for nonmagnetic neutron stars more than a few tens of years old. This scaling relation makes it possible to compare envelope results obtained by different groups using various approximations for the physical input. In § VIII it was shown that envelope calculations can be a major source of the differences among the cooling calculations of different workers, a fact not previously appreciated, since the calculations were performed for different neutron star models and hitherto not directly compared.

Using the LA radiative and conductive opacities at low densities and the recent YU calculations of the conductive opacity at high densities, we found (§ IV) that to a very good degree of approximation T_b is related to T_s/g_s by the expression $T_b = 1.288(T_s/g_s)^{0.455}$. Investigation of the sensitivity of the $T_b - T_s$ relation to small changes in the opacity shows (§ VII) that the most important input for the opacity is the conductive opacity of matter in the region where the ions are in the liquid phase. In this region the calculations of YU for the conductive opacity give values which are 2–3 times the values obtained by FI, which have been used in many recent calculations of neutron star cooling. Recent work by other investigators (Nandkumar and Pethick 1982) has now confirmed that the YU calculations are more accurate than the earlier calculations of FI. For a given T_b it is found (§ VII) that the luminosities obtained with the YU opacities are about 0.4–0.5 times the values

found using FI results. This is in good agreement with estimates obtained by using the results of our opacity sensitivity tests and the differences between the YU and FI opacities in the region where the energy transport is by thermal conduction (§ VII).

The general scaling relation between T_b and T_s^4/g_s is used in § V to relate the luminosities of different neutron star models, and in § VI it is shown how one can obtain the fully general relativistic $T_b - T_s$ relation from envelope calculations performed in the Newtonian and semirelativistic approximations.

We wish to thank Naoki Itoh, Don Lamb, Fred Lamb, Sachiko Tsuruta, V. A. Urpin, Ken Van Riper, and D. G. Yakovlev for valuable discussions and correspondence. We are grateful to W. Huebner for helpful correspondence on the Los Alamos calculations, and to R. C. Malone for sending us a copy of his thesis. The research was supported in part by NASA grant NSG-7653.

REFERENCES

- Bahcall, J. N. 1978, *Ann. Rev. Astr. Ap.*, **16**, 241.
 Baym, G., and Pethick, C. J. 1979, *Ann. Rev. Astr. Ap.*, **17**, 415.
 Baym, G., Pethick, C. J., and Sutherland, P. G. 1971, *Ap. J.*, **170**, 299.
 Bethe, H. A., and Johnson, M. B. 1974, *Nucl. Phys.*, **A230**, 1.
 Carr, W. J. 1961, *Phys. Rev.*, **122**, 1437.
 Chiu, H. Y., and Salpeter, E. E. 1964, *Phys. Rev. Letters*, **12**, 413.
 Clayton, D. D. 1968, *Principles of Stellar Evolution and Nucleosynthesis* (New York: McGraw-Hill).
 Cox, J. P., and Giuli, R. T. 1968, *Principles of Stellar Structure* (New York: Gordon & Breach).
 Eggleton, P. P., Faulkner, J., and Flannery, B. P. 1973, *Astr. Ap.*, **23**, 325.
 Epstein, R. I., Gudmundsson, E. H., and Pethick, C. J. 1983, *M.N.R.A.S.*, in press.
 Flowers, E. G., and Itoh, N. 1976, *Ap. J.*, **206**, 218.
 Glen, G., and Sutherland, P. G. 1980, *Ap. J.*, **239**, 671.
 Gudmundsson, E. H. 1981, licentiate thesis, University of Copenhagen. (Available as a Nordita Report.)
 Gudmundsson, E. H., Pethick, C. J., and Epstein, R. I. 1982, *Ap. J. (Letters)*, **259**, L19.
 Hansen, J. P. 1973, *Phys. Rev.*, **A8**, 3096.
 Harnden, F. R., Jr., et al. 1979a, *Bull. AAS*, **11**, 789.
 Harnden, F. R., Jr., Hertz, P., Gorenstein, P., Grindlay, J., Schreier, E., and Seward, F. D. 1979b, *Bull. AAS*, **11**, 424.
 Helfand, D. J. 1981a, in *X-Ray Astronomy with the Einstein Satellite*, ed. R. Giacconi (Dordrecht: Reidel), p. 39.
 ———. 1981b, in *IAU Symposium 95, Pulsars*, ed. W. Sieber and R. Wielebinski (Dordrecht: Reidel), p. 343.
 Helfand, D. J., Chanan, G. A., and Novick, R. 1980, *Nature*, **283**, 337.
 Hubbard, W. B., and Lampe, M. 1969, *Ap. J. Suppl.*, **18**, 297.
 Huebner, W. F., Merts, A. L., Magee, N. H., Jr., and Argo, M. F. 1977, *Astrophysical Opacity Library* (Rept. No. LA 6760M, Los Alamos Scientific Lab.).
 Kindl, C., and Straumann, N. 1981, *Helvetica Phys. Acta*, **54**, 214.
 Malone, R. C. 1974, Ph.D. thesis, Cornell University.
 Maxwell, O. V. 1979, *Ap. J.*, **231**, 201.
 Maxwell, O. V., and Weise, W. 1976, *Phys. Letters*, **62B**, 159.
 Mestel, L. 1950, *Proc. Cambridge Phil. Soc.*, **46**, 331.
 Morton, D. C. 1964, *Nature*, **201**, 1308.
 Murray, S. S., Fabbiano, G., Fabian, A. C., Epstein, A., and Giacconi, R. 1979, *Ap. J. (Letters)*, **234**, L69.
 Nandkumar, R., and Pethick, C. J. 1982, unpublished research.
 Nomoto, K., and Tsuruta, S. 1981, *Ap. J. (Letters)*, **250**, L19.
 Pandharipande, V. R. 1971, *Nucl. Phys.*, **A178**, 123.
 Pandharipande, V. R., and Smith, R. A. 1975a, *Nucl. Phys.*, **A237**, 507.
 ———. 1975b, *Phys. Letters*, **59B**, 15.
 Pollock, E. L., and Hansen, J. P. 1973, *Phys. Rev.*, **A8**, 3110.
 Pye, J. P., Pounds, K. A., Rolf, D. P., Seward, F. D., Smith, A., and Willingale, R. 1981, *M.N.R.A.S.*, **194**, 569.
 Rappaport, S., and Joss, P. C. 1981, in *X-Ray Astronomy with the Einstein Satellite*, ed. R. Giacconi (Dordrecht: Reidel), p. 123.
 Ray, A. 1981, *Nucl. Phys.*, **A356**, 523.
 Richardson, M. B. 1980, Ph.D. thesis, State University of New York at Albany.
 Richardson, M. B., Van Horn, H. M., Ratcliff, K. F., and Malone, R. C. 1982, *Ap. J.*, **255**, 624.
 Salpeter, E. E. 1961, *Ap. J.*, **134**, 669.
 Schwarzschild, M. 1958, *Structure and Evolution of the Stars* (Princeton: Princeton University Press).
 Shaviv, G., and Kovetz, A. 1972, *Astr. Ap.*, **16**, 72.
 Slattery, W. L., Doolen, G. D., and DeWitt, H. E. 1980, *Phys. Rev.*, **A21**, 2087.
 Soyeur, M., and Brown, G. E. 1979, *Nucl. Phys.*, **A324**, 464.
 Taylor, J. H., Fowler, L. A., and McCulloch, P. M. 1979, *Nature*, **277**, 437.
 Thorne, K. S. 1967, in *High Energy Astrophysics*, ed. C. DeWitt, E. Schatzman, and P. Véron (New York: Gordon & Breach), p. 166.
 Tsuruta, S. 1964, Ph.D. thesis, Columbia University.
 ———. 1974, in *IAU Symposium 53, Physics of Dense Matter*, ed. C. J. Hansen (Dordrecht: Reidel), p. 209.
 ———. 1979, *Phys. Rept.*, **56**, 237.
 ———. 1980, in *X-Ray Astronomy*, ed. R. Giacconi and G. Setti (Dordrecht: Reidel), p. 73.
 ———. 1981a, in *IAU Symposium 95, Pulsars*, ed. W. Seiber and R. Wielebinski (Dordrecht: Reidel), p. 331.
 ———. 1981b, private communication.
 Tsuruta, S., and Cameron, A. G. W. 1966, *Canadian J. Phys.*, **44**, 1863.
 Tuohy, I., and Garmire, G. 1980, *Ap. J. (Letters)*, **239**, L107.
 Urpin, V. A., and Yakovlev, D. G. 1979, *Astrofizika*, **15**, 647.
 ———. 1980, *Soviet Astr.*, **24**, 126.
 Van Riper, K. A. 1982, private communication.
 Van Riper, K. A., and Lamb, D. Q. 1981, *Ap. J. (Letters)*, **244**, L13.
 Weaver, T. A., Zimmerman, G. B., and Woosley, S. E. 1978, *Ap. J.*, **225**, 1021.
 Yakovlev, D. G., and Urpin, V. A. 1980, *Soviet Astr.*, **24**, 303.

R. I. EPSTEIN: Los Alamos National Laboratory, Earth and Space Sciences, MS436, Los Alamos, NM 87545

E. H. GUDMUNDSSON: Science Institute, University of Iceland, Dunhaga 3, 107 Reykjavík, Iceland

C. J. PETHICK: Department of Physics, University of Illinois at Urbana-Champaign, 1110 W. Green St., Urbana, IL 61801